ELSEVIER

Physica D 96 (1996) 162–181

PHYSICA D

Generalized scaling in fully developed turbulence

R. Benzi [a,*], L. Biferale [a], S. Ciliberto [b], M.V. Struglia [a], R. Tripiccione [c]

[a] *Dipartimento di Fisica, Universitá "Tor Vergata", Via della Ricerca Scientifica 1, I-00133 Roma, Italy*

[b] *Ecole Normale Supérieure de Lyon Laboratoire de Physique, C.N.R.S. URA1325, 46 Allée d'Italie, 69364 Lyon, France*

[c] *INFN, Sezione di Pisa, S. Piero a Grado, 50100 Pisa, Italy*

Abstract

In this paper we report numerical and experimental results on the scaling properties of the velocity turbulent fields in several flows. The limits of a new form of scaling, named Extended Self-Similarity (ESS), are discussed. We show that, when a mean shear is absent, the self-scaling exponents are universal and they do not depend on the specific flow (3D homogeneous turbulence, thermal convection, MHD). In contrast, ESS is not observed when a strong shear is present. We propose a generalized version of self-scaling which extends down to the smallest resolvable scales even in cases where ESS is not present. This new scaling is checked in several laboratory and numerical experiments. A possible theoretical interpretation is also proposed. A synthetic turbulent signal having most of the properties of a real one has been generated.

1. Introduction

In order to characterize the statistical properties of fully developed turbulence [1], one usually studies the scaling properties of moments of velocity differences at the scale r:

$$S_P(r) = \langle |v(x+r) - v(x)|^p \rangle = \langle |\delta v(r)|^p \rangle, \quad (1)$$

where $\langle \cdots \rangle$ stands for ensemble average and v is the velocity component parallel to r. At high Reynolds number, $\mathrm{Re} = U_0 L/\nu$, the $S_p(r)$ satisfies the relation

$$S_p(r) \propto r^{\zeta(p)} \quad (2)$$

for $L > r \gg \eta_k$ where L is the integral scale, $\eta_k = (\nu^3/\varepsilon)^{1/4}$ is the dissipative (Kolmogorov) scale, ε is the mean energy dissipation rate, ν the kinematic viscosity and U_0 the rms velocity of the flow. The range of length $L > r \gg \eta_k$, where the scaling relation (2) is observed, is called the inertial range. The Kolmogorov (K41) theory [2] predicts $\zeta(p) = p/3$, but experimental [3] and numerical [4] results show that $\zeta(p)$ deviates substantially from the linear law. This phenomenon is believed to be produced by the intermittent behavior of the energy dissipation [5] which can be taken into account by rewriting Eq. (2) in the following way:

$$S_p(r) \propto \langle \varepsilon_r^{p/3} \rangle r^{p/3} \propto r^{\tau(p/3)+p/3}, \quad (3)$$

where ε_r is the average of the local energy dissipation $\varepsilon(x)$ on a volume of size r centered on a point x. A comparison of Eqs. (1) and (3) leads to the conclusion that the scaling exponents $\tau(p/3)$ of the energy dissipation are related to those of S_p by $\zeta(p) = \tau(p/3) + p/3$.

* Corresponding author.

PII S0167-2789(96)00018-8

Since the Kolmogorov (K62) theory [5], many other models [6–12] have been suggested to describe the behavior of the $\zeta(p)$. However, it turns out that the $\zeta(p)$ may not be universal in nonhomogeneous, anisotropic flow and may depend on the location where measurements are done. Specifically, they may have different values if one measures either far away from boundaries where turbulence is almost homogeneous and isotropic, or in locations of the flow where a strong mean shear is present. The $\zeta(p)$ also depends on the way in which turbulence is produced, for example 3D homogeneous turbulence, boundary layer turbulence, thermal convection and MHD. Thus, there is the fundamental question of understanding in which way all these parameters influence the scaling laws. Furthermore, all the above mentioned models assume the existence of two well-defined intervals of lengths which are the inertial and dissipation ranges. According to idea of multiscaling these two ranges may eventually be connected by an intermediate region where the viscosity begins to act [13]. However, this idea of a well-defined inertial range, where viscosity does not act at all, and the idea of multiscaling turns out to be incompatible with the recently introduced new form of scaling, which has been named Extended Self-Similarity (ESS) [14,15] (see Section 2).

The ESS has been observed in 3D homogeneous and isotropic turbulence both at low and high Re and for a wide range of scales r with respect to scaling (2). In contrast, the ESS is not observed when a strong mean shear is present [16]. All these experimental observations also show that the mechanisms by which energy is actually dissipated in a flow are very poorly understood. Specifically one would like to understand how viscosity acts on different scales. This is clearly an important point in order to safely use large eddy simulations in real applications.

The purpose of this paper is to rationalize all the above mentioned results on scaling both in presence and absence of a shear. We propose a generalized form of ESS which has been checked in many different flows. We have also generated a signal which has all the statistical properties of a real turbulent signal. Our interpretation of ESS and this generalized scaling suggests that there is no sharp viscous cutoff in the intermittent transfer of energy.

The paper is organized as follows: in Section 2 we recollect the properties of ESS, in Section 3 we discuss the systems where the ESS is not observed, in Section 4 the hierarchy of structure functions is described, in Section 5 the generalized form of scaling is discussed, in Section 6 a possible theoretical interpretation is proposed and in Section 7 we discuss the multiscaling. Finally conclusions are given in Section 8.

2. Extended self-similarity

The ESS is a property of velocity structure functions of homogeneous and isotropic turbulence [14,15]. It has been shown using experimental and numerical data [17] that the structure functions present an extended scaling range when one plots one structure function against the other, namely

$$S_n(r) \propto S_m(r)^{\beta(n,m)}, \tag{4}$$

where $\beta(n, m) = \zeta(n)/\zeta(m)$. The details of ESS have been reported elsewhere [15]. In the following we describe only the main features.

As an example we consider two experimental data sets at different R_λ, which is the Reynolds number based on the Taylor scale ($R_\lambda \simeq 1.4\,\mathrm{Re}^{1/2}$) [1]. The two experiments are a jet at $R_\lambda = 800$ and the wake behind a cylinder at $R_\lambda = 140$. In both cases data have been recorded at about 25 integral scales downstream [15]. In Fig. 1(a) $S_6/r^{\zeta(6)}$, computed for the two experiments, is plotted as a function of r. In Fig. 1(b) we show $S_3/r^{\zeta(3)}$ as a function of r. In both figures a scaling region is observed only for the highest R_λ. In constrast if the relative scaling (4) is used, see Fig. 2, a clear scaling is present for both R_λ with $\beta(6, 3) \cong 1.78$. The vertical dashed lines in the Fig. 2 correspond to $r = 5\eta_k$ and they roughly indicate the extension of the scaling (4), that is $5\eta_k < r < L$.

The ESS scaling has been checked both on numerical data and in experiments, in a range $30 < R_\lambda <$

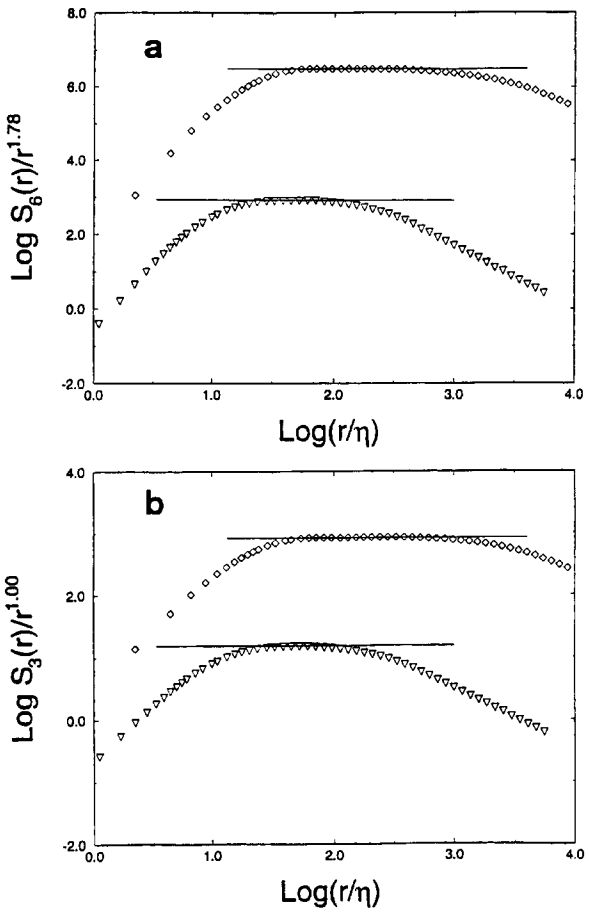

Fig. 1. Structure functions $S_p(r)/r^{\zeta(p)}$ as a function of r. Data taken from an experiment on a jet at $R_\lambda = 800$ ($\diamond$). Data taken from the wake behind a cylinder at $R_\lambda = 140$ ($\triangle$). (a) $p = 6$ and $\zeta(6) = 1.78$, (b) $p = 3$ and $\zeta(3) = 1$. Logarithms are base 10 in all of the figures if not otherwise indicated.

2000. A direct consequence of the scaling (4) is that for all p, S_p can be written in the following way:

$$S_p(r) = C_p U_0^p \left[\frac{r}{L} f\left(\frac{r}{\eta_k}\right)\right]^{\zeta(p)} \tag{5}$$

with $U_0^3 = S_3(L)$, $L = U_0^3/\varepsilon$ being the integral scale and C_p dimensionless constant selected in such a way that $f(x) = 1$ for $x \gg 1$. Eq. (5) has been carefully checked by computing the function

$$f_p\left(\frac{r}{\eta_k}\right) = \frac{L}{r}\left(\frac{S_p(r)}{C_p U_0^p}\right)^{1/\zeta(p)}$$

If f_p is independent of p, then Eq. (5) is satisfied.

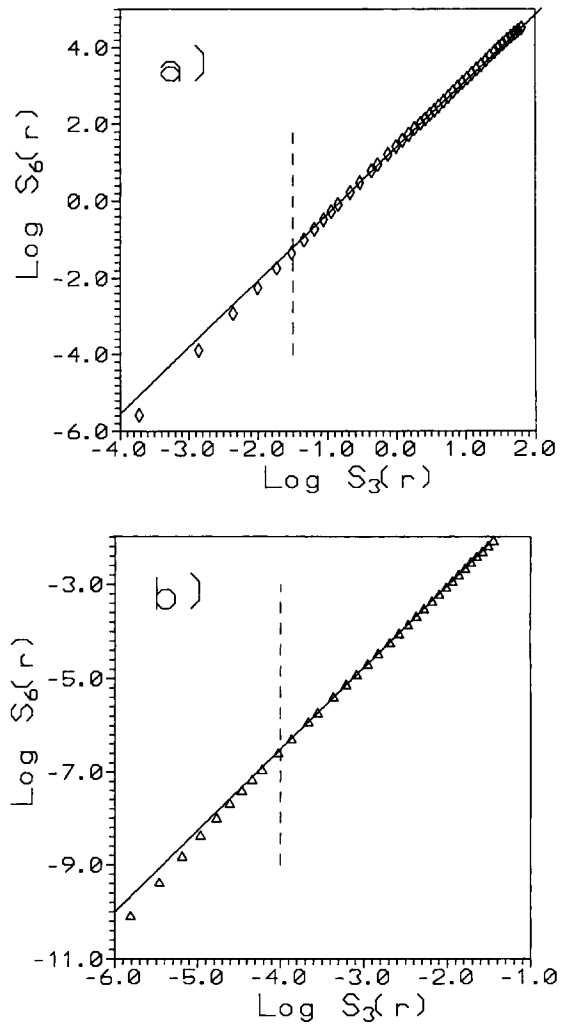

Fig. 2. Structure functions S_6 as a function of S_3 at $R_\lambda = 800$ (a) and $R_\lambda = 140$ (b), computed from the same data set of Fig. 1. Vertical dashed lines indicate the value of S_3 at $5\eta_k$.

This is seen in Fig. 3 where $\log(f_6/f_2)$ and $\log(f_4/f_2)$ are plotted as a function of r/η_k. We clearly see that both the ratios are close to 1 within 2% for $r > 5\eta_k$. This result shows that Eq. (4) is satisfied for $5\eta_k < r < L$.

The ESS has been also checked for the temperature and velocity fields in Rayleigh–Benard convection [18] and in the case of a passive scalar [19]. It turns out that the ESS is a very useful tool in order to distinguish between Kolmogorov and Bolgiano scalings [18,20]. Let us briefly remind the basic properties of Bolgiano scaling for Rayleigh–Benard convection.

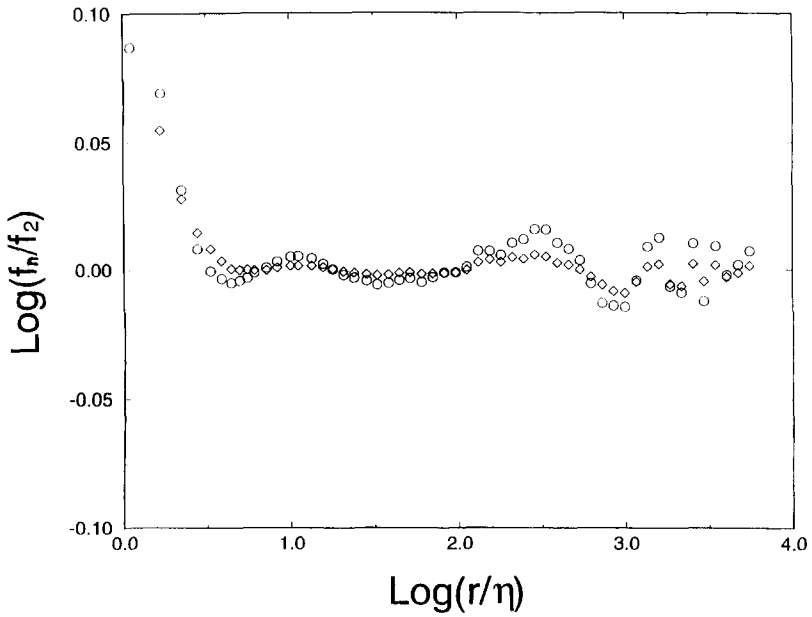

Fig. 3. Logarithm of ratio of the universal functions f_n/f_2 for two cases $n = 6$ ($\diamond$) and $n = 4$ ($\circ$) for the wake behind the cylinder of Fig. 1 as a function of r/η_k.

By assuming that the Boussinesq approximation holds, one can introduce the Bolgiano scale

$$L_B = \frac{\varepsilon^{5/4}}{(g\alpha)^{3/2}N^{3/4}}, \tag{6}$$

where ε is the mean rate of energy dissipation, α is the thermal expansion coefficient, g is the gravity acceleration and N is the rate of temperature dissipation. The Bolgiano scaling can be deduced by the exact scaling relation $\langle \delta v(r)\delta T^2(r)\rangle \sim Nr$, where $\delta v(r) = v(x+r) - v(x)$ and $\delta T(r) = T(x+r) - T(x)$, and by the balance between thermal forcing and nonlinear velocity advection

$$\delta v^2(r) \sim g\alpha\delta T(r)r. \tag{7}$$

It follows that, disregarding intermittency

$$\delta v(r) \sim (g\alpha)^{2/5}N^{1/5}r^{3/5}, \tag{8}$$

$$\delta T(r) \sim (g\alpha)^{-1/5}N^{2/5}r^{1/5}. \tag{9}$$

One can show that the Bolgiano scaling should be observed only for $r > L_B$ [1,18]. For $r < L_B$ the usual Kolmogorov scaling is recovered [18].

In the case of the Bolgiano scaling it has been found that $\zeta(3) = 2.08$ which is clearly very different from the Kolmogorov value $\zeta(3) = 1$. In spite of this large difference between the values of the exponent $\zeta(3)$, using ESS one discovers that the ratio $\zeta(p)/\zeta(3)$ in the case of Bolgiano are equal to those of homogeneous and isotropic turbulence. The same property is observed for the $\zeta(p)$ obtained from measurements done on the solar wind [21]. In Table 1 we compare the $\zeta(p)$ measured in different physical systems and the ratios $\beta(p, 3)$ for MHD and Rayleigh–Benard convection.

Another interesting observation concerns the behavior of $\beta(p, 3)$ with respect to R_λ. The values of $\beta(p, 3)$ reported in Table 1 have been measured in the range $30 < R_\lambda < 5 \times 10^6$. First we note that, within error bars, any change or trend of $\beta(p, 3)$ as a function of R_λ is absent. Second, we show in Fig. 4 the dependence of $\beta(6, 3)$ on R_λ (a similar result has been reported in Ref. [22]). This means that far away from boundaries, the $\beta(p, 3)$ are constants which do not depend on Re and on the way in which turbulence has been generated.

A final point regarding ESS, concerns the generalization of the Refined Kolmogorov Similarity Hypothesis (RKSH).

Table 1
We show some measured values of $\zeta(p)$ and $\beta(p,3)$ for $1 \le p \le 8$.

p	ζ_p	ζ_p (Bolg.)	ζ_p (MHD)	$\beta(p,3)$ (Bolg.)	$\beta(p,3)$ (MHD)
1	0.37	0.77	0.28	0.37	0.36
2	0.70	1.46	0.55	0.70	0.70
3	1.00	2.08	0.78	1.00	1.00
4	1.28	2.66	1.00	1.28	1.28
5	1.54	3.20	1.20	1.54	1.54
6	1.78	3.70	1.39	1.78	1.78
7	2.00	4.16	1.58	2.02	2.02
8	2.23	4.63	1.75	2.24	2.24

Note: In the second column we report the $\zeta(p)$ measured in 3D homogeneous and isotropic turbulence ($30 < R_\lambda < 2000$), in the third column the $\zeta(p)$ measured in Rayleigh–Benard convection when the Bolgiano scaling is the relevant one ($R_\lambda \simeq 30$), in the fourth column the $\zeta(p)$ obtained from the measurements of the solar wind ($R_\lambda \simeq 5 \times 10^6$). We note that the $\zeta(3)$ of the last two cases are clearly very different from 1 which is the value of $\zeta(3)$ in the second column. The ratios $\beta(p,3)$ computed from the values of the third and fourth column are shown in the fifth and sixth columns, respectively. The $\beta(p,3)$ are equal within error bars to those of the first column.

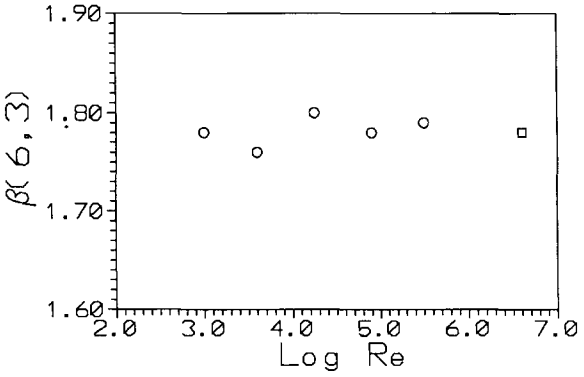

Fig. 4. Dependence of the exponent $\beta(6,3)$ as a function of $\log_{10}$ Re. ($R_\lambda \simeq 1.4\,\mathrm{Re}^{1/2}$.) The last point is from Ref. [3]. See also Ref. [22].

The RKSH states that $\varepsilon_r \sim \delta v^3/r$, as far as the dependence on the scale r is concerned and supports Eq. (3). We can generalize the RKSH by introducing an effective scale $L(r) = S_3(r)/\varepsilon$, as suggested by ESS, and we obtain the following relation: $\varepsilon_r = \delta v^3 \varepsilon / S_3$.

Generalization of RKSH simply states that

$$S_p(r) = \langle |\delta v(r)^p| \rangle = \frac{\langle \varepsilon_r^{p/3} \rangle}{\varepsilon^{p/3}} S_3(r)^{p/3}. \tag{10}$$

In Section 6 we give some theoretical support of Eq. (10).

Eq. (10) has been first proposed in Ref. [15] and carefully checked in Ref. [23]. A typical experimental

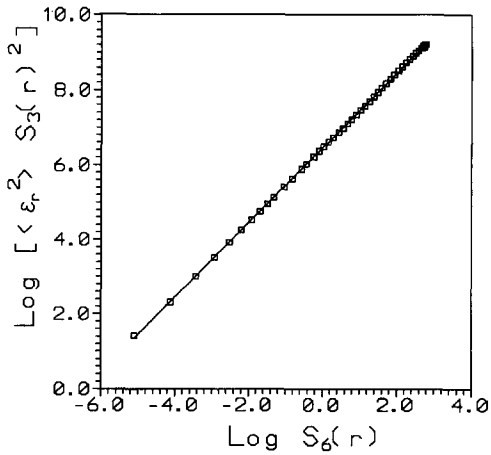

Fig. 5. Log–log plot of $\langle \varepsilon_r^2 \rangle S_3(r)^2$ against $S_6(r)$ at $R_\lambda = 500$. The straight line refers to the slope 1.005. Data are from an experiment of turbulence behind a cylinder and the measurement point was at about 25 diameter down stream.

result is shown in Fig. 5 where $\langle \varepsilon^2 \rangle S_3^2$ is plotted as a function of $S_6(r)$. The energy dissipation has been computed using the 1D surrogate that is

$$\varepsilon_r = \frac{\nu}{r} \int_x^{x+r} \left(\frac{\partial V(x')}{\partial x} \right)^2 \mathrm{d}x'. \tag{11}$$

In Fig. 5 one can see a clear scaling extending over almost ten decades from the integral scale to η_k. The slope of the straight line is 1.005 showing that Eq. (10) is compatible with experimental data.

One can argue that Eq. (10) is a trivial one because for $r < \eta_k$, ε_r is constant and $S_p \propto r^p$, thus the scaling $S_n \propto S_3^{p/3}$ is obviously satisfied. Furthermore, for r in the inertial range Eq. (10) is certainly verified because $(S_3/\varepsilon) \propto r$. However, in principle the proportionality constant of Eq. (10) in the inertial and in the dissipative range could be different. The fact that experimentally they are found equal has several important consequences which will be discussed in Section 5.

3. Systems where ESS is not observed

In Section 2 we have discussed several systems where not only the ESS works but also the exponents $\beta(n, 3)$ are universal because they do not depend on the systems and on Re. We want to stress that this kind of universality, observed in different flows, disappears if the system is influenced by the presence of a strong mean shear. In this case ESS does not work, because an extended range of scaling is not present when S_n is drawn as a function of S_3. Violation of ESS has been observed experimentally in boundary layer turbulence [16,24] and in the shear behind a cylinder [25].

In a recent numerical simulation [26] the effect of the shear on scaling laws has been carefully investigated using a Kolmogorov flow. This simulation concerns a 3D fluid occupying a volume of $V = L^3$ sites with $L = 160$, and forced such that the stationary solution has a nonzero spatial dependent mean velocity $\langle v(x) \rangle = \boldsymbol{x} \sin(8\pi z/L)$, where $\boldsymbol{x}$ is the versor in the direction x, and L is the integral scale. In Fig. 6(a) and (b) we show the standard ESS analysis by plotting $\log(S_6)$ as a function of $\log(S_3)$ for two specific levels z_a and z_b, where z_a and z_b were chosen at the level of minimum and maximum shear respectively. The R_λ of the simulation was 40 and no scaling laws were present if examined as a function of r.

Nevertheless, it is clear from Fig. 6(a) that ESS is observed for the case of minimum shear and it is not observed for the case of maximum shear (Fig. 6(b)). In both figures, the dashed lines are the best fit done in the range between the 20th and 30th grid point and correspond to the slopes $\beta(6, 3) = 1.78$ and $\beta(6, 3) = 1.43$ for the minimum and maximum shear, respectively.

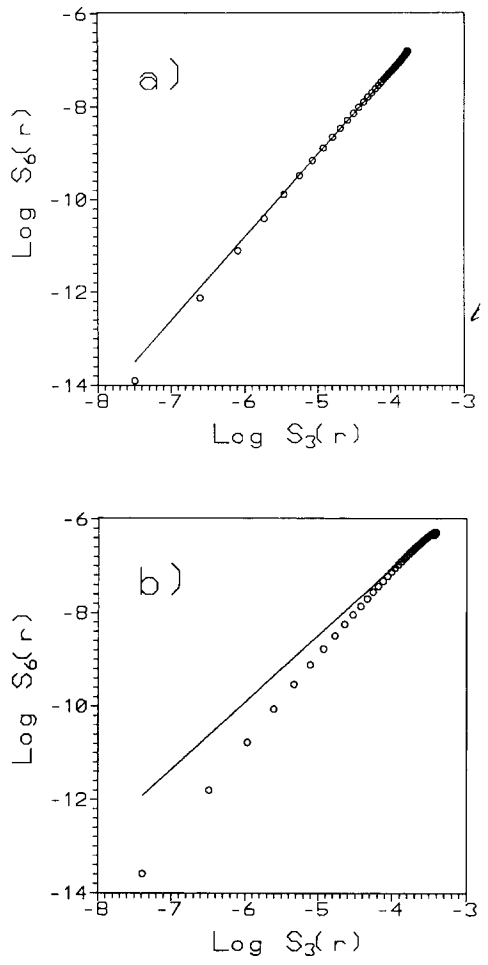

Fig. 6. (a) Log–log plot of ESS scaling for the longitudinal structure function $S_6(r)$ versus $S_3(r)$. Data are taken from a numerical simulation of a shear flow at $R_\lambda = 40$. The dashed line is the best fit with slope 1.79. Every point in the plot corresponds to a grid point and the lattice spacing is $\sim 1\eta_k$ wide. The computation of the structure functions is performed in points of the flow where the shear has a minimum. (b) the same of (a) but for points where the shear is maximum. The dashed line is the best fit with slope 1.43. At variance with previous case ESS is not observed.

However, one finds that generalized Kolmogorov similarity hypothesis Eq. (10) is satisfied also for values of r where ESS is no longer satisfied. In order to highlight the previous comment, we consider again the above mentioned Kolmogorov flow. In Fig. 7(a) and (b) we show the result of the scaling obtained by using Eq. (10) at the correspondent z-levels of Fig. 6(a) and (b) for $p = 6$. As one can see the generalized

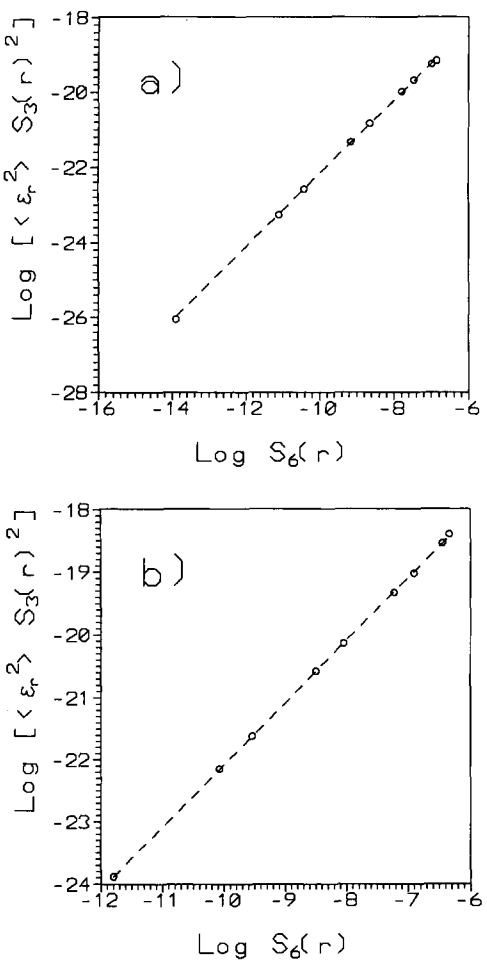

Fig. 7. Check of Eq. (10) for $p = 6$ using the same numerical simulation of the shear flow discussed in Fig. 6 (log–log plot). Energy dissipation has been computed by using the 1D surrogate in order to compare this result with laboratory experiments (see Fig. 5). (a) Points of minimum shear, (b) points of maximum shear. The points refer to the scales at 2, 4, 5, 8, 10, 16, 20, 32, 40 grid points and the dashed line is the best fit done over these points, corresponding to the slope 0.99 for both minimum and maximum shear data. Although in this case ESS is not observed (see Fig. 6(b)), the generalized refined Kolmogorov hypothesis Eq. (10) works within 3%.

Kolmogorov similarity hypothesis is well satisfied in both cases although for z_b ESS is not observed. This is another important experimental and numerical result which we will consider again in Section 5.

The other relationship which we have observed to hold from large to small scales even in absence of ESS is the moment hierarchy recently proposed in Ref. [12] and rewritten in terms of velocity structure functions in Ref. [27].

4. Hierarchy of structure functions

In a recent letter [12] She and Leveque have proposed an interesting theory to explain the anomalous scaling exponents of velocity structure functions. The theory yields a prediction

$$\zeta(p) = p/9 + 2(1 - (2/3)^{p/3}),$$

which is in very good agreement with available experimental data [15].

The She–Leveque model is based upon the fundamental assumption on the hierarchy of the moments, $\langle \varepsilon_r^n \rangle$, of the local energy dissipation. Specifically they consider that

$$\frac{\langle \varepsilon_r^{n+1} \rangle}{\langle \varepsilon_r^n \rangle} = A_n \left(\frac{\langle \varepsilon_r^n \rangle}{\langle \varepsilon_r^{n-1} \rangle} \right)^{\beta} (\varepsilon_r^{(\infty)})^{(1-\beta)}, \tag{12}$$

where A_n are geometrical constants and $\varepsilon_r^{(\infty)} = \lim_{n\to\infty}(\langle \varepsilon_r^{n+1} \rangle / \langle \varepsilon_r^n \rangle)$ is associated in Ref. [12] with filamentary structures of the flow. On the basis of simple arguments it is assumed that $\varepsilon_r^{(\infty)} \propto r^{-2/3}$. The value of β predicted in Ref. [12] is $\frac{2}{3}$. Notice that in Eq. (12) for $n = 1$, taking into account that $\langle \varepsilon_r \rangle = \varepsilon$ is constant in r, one immediately finds that

$$(\varepsilon_r^{(\infty)})^{(1-\beta)} \propto \langle \varepsilon_r^2 \rangle = S_6/S_3^2, \tag{13}$$

where Eq. (10) has been used.

Eq. (12), which has been experimentally tested in Ref. [28], can be extended to the velocity structure functions [27]. Taking in Eq. (12) the value $n = \frac{1}{3}p$ and using Eqs. (10) and (13) after some algebra one finds the following relation for the velocity structure functions:

$$F_{p+1}(r) = C_p (F_p(r))^{\beta'} \cdot \tilde{F}(r), \tag{14}$$

where

$$F_{p+1}(r) = \frac{S_{p+1}(r)}{S_p(r)}$$

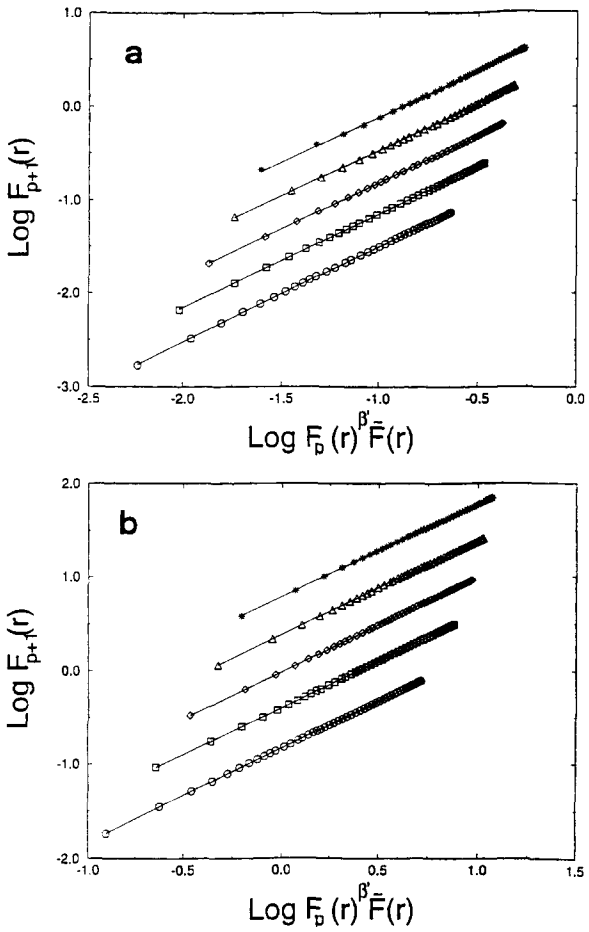

Fig. 8. The function $F_{p+1}(r)$ defined in Eq. (14) is plotted, for several values of p, as a function of $[(F_p(r))^{\beta'} \cdot \tilde{F}(r)]$ with $\beta = \frac{2}{3}$, $\beta' = \beta^{\delta}$ and $\delta = \frac{1}{3}$. $R_\lambda = 140$ in (a) and $R_\lambda = 800$ in (b). The five curves in (a) and (b) correspond to $p = 1, 2, 3, 4, 5$ starting from the bottom lines. They have been vertically shifted of $-0.4, -0.2, 0, 0.2, 0.4$ in order to separate them. The solid lines have slope 1.

and

$$\tilde{F}(r) = \left(\frac{S_6}{S_3^{(1+\beta)}}\right)^{(1-\beta')/3(1-\beta)},$$

C_p are geometry dependent constants and $\beta' = \beta^{1/3}$.

Notice that Eq. (14) is certainly valid for any β in the dissipative range where $S_n \propto r^n$. Eq. (14) has been experimentally tested in Ref. [27].

This can be seen in Fig. 8(a) and (b) where the scaling obtained for various p using Eq. (14) is reported for two different Re. As we have already observed in the case of Eq. (10) (Fig. 5), the scaling extends from large to small scales even for values of r where ESS is no longer satisfied. It is important to point out that the validity of (14) for all scales is not necesserily true for any turbulent field, but it is an important feature of the velocity field. As an example, in Appendix A we show that the passive scalar field does not present the same property.

5. A generalized form of ESS

In Sections 3 and 4 we have shown that the Generalization of Kolmogorov Refined Similarity hypothesis (GKRS) Eq. (10) and the hierarchy of moments Eq. (14) are two relations which are satisfied even in flows where ESS is not observed. These results suggest that the concept of ESS could be generalized in such a way to take into account the scaling relations Eqs. (10) and (14) properly.

For this purpose we introduce the dimensionless structure function

$$G_p(r) = \frac{S_p(r)}{S_3(r)^{p/3}}. \tag{15}$$

According to Kolmogorov theory (15) should be a constant both in the inertial and in the dissipative range, although the two constants are not necessarily the same. Because of the presence of anomalous scaling, $G_p(r)$ are no longer constants and by using (10) we have

$$G_p(r) = \langle \varepsilon_r^{p/3} \rangle. \tag{16}$$

Thus the functions $G_p(r)$ satisfy the hierarchies (12) and (14). Following the results of Sections 3 and 4, Eq. (16) is valid for all scales even in cases where ESS is not verified. Therefore, it seems reasonable to study the self-scaling properties of $G_p(r)$ or, equivalently, the self-scaling properties of the energy dissipation averaged on an interval of size r,

$$G_p(r) = G_q(r)^{\rho(p,q)}, \tag{17}$$

where we have by definition

$$\rho(p, q) = \frac{\zeta(p) - p/3\ \zeta(3)}{\zeta(q) - q/3\ \zeta(3)}. \tag{18}$$

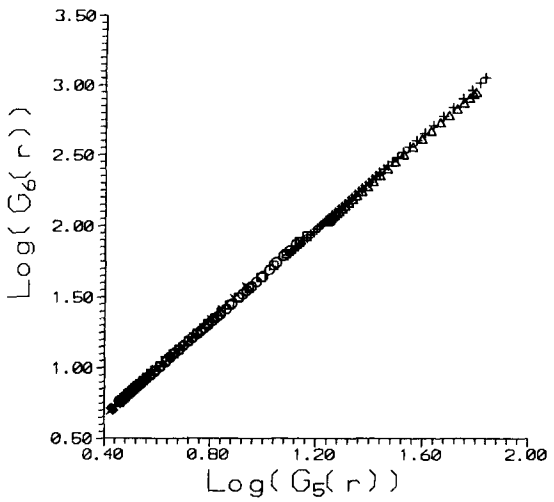

Fig. 9. Log–log plot of $G_6(r)$ versus $G_5(r)$ for different laboratory and numerical experiments. (+) Data are taken in a wake behind a cylinder where standard ESS was not observed [25]. (o) Data taken from the region with log-profile of a boundary layer (courtesy of G. Ruiz Chavarria) where standard ESS was not observed. (□) Data taken from a numerical simulation of thermal convection [18] where standard ESS was observed. (Δ) Data taken from a direct numerical simulation of a channel flow where standard ESS was not observed [29].

$\rho(p,q)$ is given by the ratio between deviations from the K41 scaling. It will play an essential role in our understanding of energy cascade. Indeed, it is easy to realize that it is the only quantity that can stay constant all along the cascade process: from the integral to the sub-viscous scales. It is reasonable to imagine that the velocity field becomes laminar in the sub-viscous range, $S_p(r) \propto r^p$, still preserving some intermittent degree parametrized by the ratio between corrections to the K41 theory. In order to check the validity of Eq. (17) we have plotted in Fig. 9 $G_6(r)$ versus $G_5(r)$ for many different experimental set-up [25,24,18,29], done at different Reynolds numbers and for some direct numerical simulation with and without large scale shear. As one can see, the straight line behavior is very well supported within experimental errors (of the order of 3%) and no deviations from the scaling regime are detected. Similar results are obtained, using different $G_p(r)$ and $G_q(r)$.

There are two alternative ways to check (17). First of all, one can rewrite it in the following way:

$$S_p(r) = (S_q(r))^{\rho(p,q)} (S_3(r))^{p/3 - r(p,q)q/3}. \tag{19}$$

If (17) is true then $\rho(p,q)$ should be equal to $r(p,q)$. One can use (19) directly and perform a two variable fit of $\rho(p,q)$ and $r(p,q)$. Then the quantity

$$\sigma_{p,q} = \frac{\rho(p,q) - r(p,q)}{\rho(p,q)} \tag{20}$$

gives a measure of the accuracy of (17). We have computed $\sigma_{p,q}$ for p and q in the range [1,8] for all the experimental and numerical results. We have found that

$$\sup_{p,q}[\sigma_{p,q}] = 0.01, \tag{21}$$

where the above test has been done over all the experimental and numerical data available to us. This result tells us that the accuracy of (17) is extremely well verified.

A second and independent check of (17) can be done by using (14). Indeed (14) can be checked either for fixed p as a function of r or for fixed r as a function of p. In the second case we may assume that the constant C_p in (14) is p-independent and, by plotting in a log–log scale F_{p+1} against F_p for fixed r and different p, we can estimate the exponent β'. If (17) is true then we should observe scaling (14) both at large scale and very small scale with the same value of β'. Let us remark that the previous statement (on which our test of (17) is based) depends on the two assumptions that the log-Poisson hierarchy for structure functions is true and that the constant C_p in (14) are p-independent. In Fig. 10(a) and (b) we show a log–log plot of F_{p+1} against F_p for $p = 1, \ldots, 6$ and $r = 3\eta_k$ and $r = 30\eta_k$ for the case of two numerical simulations, namely Rayleigh–Bernard thermal convection and channel flow. As one can see, a clear scaling is observed with the same scaling exponent β' both for small and relatively large values of r. This confirms the quality of the generalized ESS scaling (17).

6. A theoretical interpretation

The aim of this section is to discuss a possible theoretical interpretation of the experimental and

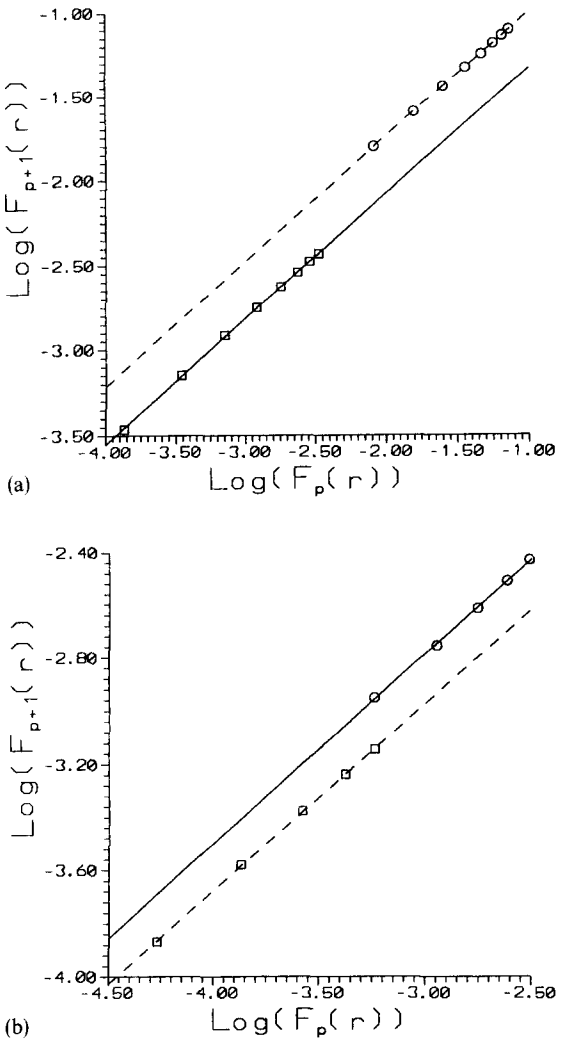

Fig. 10. Log–log plot of F_{p+1} against F_p for $p = 1, \ldots, 6$ and $r = 3\eta_k$ (□) and $r = 30\eta_k$ (○) for the case of two numerical simulations, namely Rayleigh–Bernard thermal convection (a) and channel flow (b). As one can see, a clear scaling is observed with the same scaling exponent β' both for small and relatively large values of r. This confirms the quality of the G-ESS scaling (17).

numerical results previously shown. Our starting point is to revise the concept of scaling in fully developed turbulence.

Let us consider three length scales $r_1 > r_2 > r_3$ and our basic variables to describe the statistical properties of turbulence, namely the velocity difference $\delta v(r_i)$. We shall restrict ourselves to those statistical models of turbulence based on random multiplier. Thus we shall assume that there exists a statistical equivalence of the form

$$\delta v(r_i) = a_{ij}\delta v(r_j), \tag{22}$$

where $r_i < r_j$ and a_{ij} is a random number with a prescribed probability distribution P_{ij}. By definition, we have

$$a_{13} = a_{12}a_{23}. \tag{23}$$

Eq. (23) is true no matter which is the ratio r_1/r_2 and r_2/r_3. Now we ask ourselves the following question: what is the probability distribution P_{ij} which is functionally invariant under the transformation (23)? This question can be answered by noting that Eq. (23) is equivalent to write:

$$\log a_{13} = \log a_{12} + \log a_{23} \tag{24}$$

(we assume $a_{ij} > 0$). Thus our question is equivalent to ask what are the probability distribution stable under convolution. For independently distributed random variables a solution of this problem can be given in a complete form [30,31]. If the variables are correlated the situation becomes much more difficult to solve, as it is well known from the theory of critical phenomena. For the time being we shall restrict ourselves to independent random variables.

In this case, for instance, the gaussian and the Poisson distributions are well-known examples of probability distribution stable under convolution. These two examples correspond to two turbulence models proposed in literature, namely the log-normal model [5] and the log-Poisson model [12,32,33,35]. A more general description can be found in [31]. The log-Poisson model implies also that the probability distribution function (PDF) of δv on the scale r is related to the large scale one via a linear relation [32,34,35]. This functional dependence of the velcoity difference PDF, which is compatible with ESS [35], has been previously proposed by Castaing and Gagne [10,11].

We can have a different point of view on our question which is fully equivalent to the above discussion (see also [35]). A simple solution to our

question is given by all probability distribution P_{ij} such that

$$\langle a_{ij}^p \rangle \equiv \prod_{k=1}^{n} \left(\frac{g_k(r_j)}{g_k(r_i)} \right)^{\gamma_k(p)} \tag{25}$$

for any functions $g_k(r_i)$ and $\gamma_k(p)$ ($\langle \cdots \rangle$ represents average over P_{ij}). Indeed we have

$$\begin{aligned} \langle a_{13}^p \rangle &= \langle a_{12}^p a_{23}^p \rangle \\ &= \prod_{k=1}^{n} \left(\frac{g_k(r_1)}{g_k(r_2)} \right)^{\gamma_k(p)} \prod_{k=1}^{n} \left(\frac{g_k(r_2)}{g_k(r_3)} \right)^{\gamma_k(p)} \\ &= \prod_{k=1}^{n} \left(\frac{g_k(r_1)}{g_k(r_3)} \right)^{\gamma_k(p)} . \end{aligned} \tag{26}$$

We want to remark that Eq. (25) represents the most general solution to our problem, independent of the scale ratio r_i/r_j.

Let us give a simple example in order to link Eq. (25) to the case of probability distribution stable under convolution. Following [12,32,33] let us consider the case of a random log-Poisson multiplicative process, namely

$$a_{ij} = A_{ij} \beta^x, \tag{27}$$

where x is a Poisson process $P(x = N) = (C_{ij}^N e^{-C_{ij}})/N!$.
By using (27) we obtain

$$\langle a_{ij}^p \rangle = A_{ij}^p \exp(C_{ij}(\beta^p - 1)). \tag{28}$$

Eq. (28) is precisely of the form (25) if we write

$$A_{ij} = \frac{g_1(r_j)}{g_1(r_i)}, \qquad \exp C_{ij} = \frac{g_2(r_i)}{g_2(r_j)}. \tag{29}$$

In order to recover the standard form of She–Leveque model we need to assume that (see also (35)):

$$g_1(r_i) \sim r_i^h, \tag{30}$$

$$g_2(r_i) \sim r_i^2. \tag{31}$$

This example highlights one important point in our discussion, i.e. the general requirement of scale-invariant random multiplier (25) does not necessarily imply a simple power-law scaling as expressed by Eqs. (30) and (31). Moreover, the general expression (25) is compatible to infinitely divisible distribution. For instance, previous random multiplier model for turbulence, such as the β-random model or the p-model, cannot be expressed in the general form (25) independently of the ratio r_i/r_j.

It is worthwhile to review the multifractal language in light of the previous discussion. In the multifractal language for turbulence, the two basic assumptions are:

(I) The velocity difference on scale r shows local scaling law with exponent h, i.e. $\delta v(r) \sim r^h$.
(II) The probability distribution to observe the scaling $\delta v(r) \sim r^h$ is given by $r^{3-D(h)}$.

In the multifractal language, therefore, there are two major ansatz: one concerns power-law scaling of the velocity difference (assumption (I)) and the other one concerns a geometrical interpretation (the fractal dimension $D(h)$) of the probability distribution to observe a local scaling with exponent h. How is it possible to generalize the multifractal language in order to take into account Eq. (25)?

As we shall see, the theory of infinitely divisible distribution is the tool we need to answer the previous question. All published models of turbulence based on infinitely divisible distribution are equivalent to write $D(h)$ in the form

$$3 - D(h) = d_0 f\left[\frac{h - h_0}{d_0} \right], \tag{32}$$

where d_0 and h_0 are the two free parameters while the function $f(x)$ depends only on the choice of the probability distribution. For instance for log-normal distribution, $f(x) = x^2$. Eq. (32) allows us to write

$$\begin{aligned} \langle \delta v(r)^p \rangle &= \int \mathrm{d}\mu(h) r^{hp} r^{3-D(h)} \\ &= r^{h_0 p + d_0 H(p)}, \end{aligned} \tag{33}$$

where

$$H(p) = \inf_x (px + f(x)). \tag{34}$$

We can see that Eq. (33) is equivalent to a random multiplicative process given by

$$\langle a_{ij}^p \rangle = \left(\frac{r_j}{r_i} \right)^{h_0 p} \left(\frac{r_j}{r_i} \right)^{d_0 H(p)} \tag{35}$$

Eq. (35) can be generalized to the form (25) by allowing h_0 and d_0 to depend on r, i.e.

$$\langle a_{ij}^p \rangle = \frac{\left(r_j^{\bar{h}_0(r_j)}\right)^p}{\left(r_i^{\bar{h}_0(r_i)}\right)^p} \left[\frac{r_j^{\bar{d}_0(r_j)}}{r_i^{\bar{d}_0(r_j)}}\right]^{H(p)}, \tag{36}$$

where

$$\bar{h}_0(r) = h_0 s_h(r), \qquad \bar{d}_0(r) = d_0 s_d(r). \tag{37}$$

Eq. (36) is equivalent to (25) by using

$$g_1(r_i) = r_i^{\bar{h}_0(r_i)}, \qquad g_2(r_i) = r_i^{\bar{d}_0(r_i)}, \tag{38}$$

$$\gamma_1(p) = p, \tag{39}$$

$$\gamma_2(p) = H(p). \tag{40}$$

The same results can be obtained by (33), i.e. we have

$$\langle \delta v(r)^p \rangle = r^{\bar{h}_0(r)p + \bar{d}_0(r)H(p)}. \tag{41}$$

Note that the saddle point evaluation of (33) is not spoiled by the dependence of h_0 and d_0 on r.

We have seen that (25) can be reformulated in terms of multifractal language for infinitely divisible distribution whose function $D(h)$ can be rewritten as in (32). We can ask the following question: what is the physical meaning of (25) or its multifractal analogous (36)–(41)? It is precisely the multifractal language which allows us to answer this question. Indeed, the two basic assumptions for the multifractal language can now be replaced in the following way:

(I) the velocity difference on scale r behaves as

$$\delta v(r) \sim g_1(r) g_2(r)^x; \tag{42}$$

(II) the probability distribution to observe (I) is $g_2(r)^{f(x)}$.

Then we have

$$\langle \delta v(r)^p \rangle = \int \mathrm{d}\mu(x) g_1(r)^p g_2(r)^{px + f(x)} = g_1(r)^p g_2(r)^{H(p)} \tag{43}$$

by employing a saddle point integration. The most clear physical interpretation of (43) is that the probability to observe a given fluctuation of the velocity difference has no more geometrical interpretation linked to the fractal dimension $D(h)$. The probability distributions are controlled by a dynamical variable $g_2(r)$ which at this stage we still need to understand. An insight on the dynamical meaning of $g_2(r)$ can be obtained by the following considerations.

Let us define $\varepsilon(r)$ the average of the energy dissipation on a scale r. We can define the eddy turnover time $\tau(r)$ on scale r as

$$\frac{\delta v^2(r)}{\tau(r)} \sim \varepsilon(r). \tag{44}$$

We have seen that all experimental and numerical data suggest that the following relation is always (see also Eq. (10) and Ref. [32]):

$$\frac{\varepsilon(r)}{\langle \varepsilon \rangle} =^s \frac{\delta v^3(r)}{\langle \delta v^3(r) \rangle}, \tag{45}$$

where $=^s$ means that all moments on the right-hand side are equal to the left-hand side. By using (44) and (45) we obtain the definition of length $L(r)$

$$L(r) \equiv \delta v(r) \tau(r) = \frac{\langle \delta v^3(r) \rangle}{\varepsilon}. \tag{46}$$

$L(r)$ cannot be regarded as a real length scale in the physical space. Rather, $L(r)$ should be considered as a dynamical variable entering into the statistical description of turbulence. This is precisely the idea behind ESS which reformulates the scaling properties of turbulence in terms of $L(r)$. Indeed in order to obtain ESS from (43) it is sufficient to state that, within the range of scales where ESS is observed, $g_1(r)^{1/h_0} \sim g_2(r)^{1/d_0} \sim L(r)$. The physical meaning of ESS is strictly linked to (46) and in particular to (45) which is a GKRS hypothesis.

Let us summarize all our previous findings.

(A) We have introduced the idea of scale invariant random multiplier satisfying Eq. (25).

(B) We have shown that infinitely divisible distributions are all compatible with (25).

(C) We have shown that the multifractal language specialized for the case of infinitely divisible distribution gives Eq. (25) (with $n = 2$ and $\gamma_1(p)$ linear in p) and it is equivalent to scale invariant random multiplier.

(D) Finally we have argued that the correct scaling parameter to describe the statistical properties of

small scale turbulent flows is not directly linked to a simple geometrical interpretation, rather it should be considered a dynamical variable.

Our findings (A)–(D) enable us to have a unified theoretical interpretation of the experimental and numerical results presented at the beginning of this paper. Indeed Eq. (41) or (43) tells us that the anomalous part of the structure functions

$$G_p(r) \equiv \frac{\langle \delta v^p(r) \rangle}{\langle \delta v^3(r) \rangle^{p/3}} \tag{47}$$

satisfies the scaling properties

$$G_p(r) = G_q(r)^{\rho_{p,q}}, \tag{48}$$

where $\rho_{p,q} \equiv (\zeta_p - p/3)/(\zeta_q - q/3)$. According to our analysis of the experimental and numerical results, the scaling (48) is observed down to the smallest resolved scale.

We have shown that, in the theoretical framework so far exposed, we recover the ESS when $g_1(r)^{1/h_0} \sim g_2^{1/d_0} \sim L(r)$. If $g_1(r)^{1/h_0} \neq g_2(r)^{1/d_0}$ we lose ESS, but its generalized version (48) is still valid.

6.1. Synthetic turbulence

We can also use (41) and (43) to simulate a synthetic signal according to a random multiplicative process satisfying (36). This can be done by using the algorithm recently introduced in [36].

Let us consider a wavelet decomposition of the function $\phi(x)$

$$\phi(x) = \sum_{j,k=0}^{\infty} \alpha_{j,k} \psi_{j,k}(x), \tag{49}$$

where $\psi_{j,k}(x) = 2^{j/2}\psi(2^j x - k)$ and $\psi(x)$ is any wavelet with zero mean. The above decomposition defines the signal as a diadic superposition of basic fluctuations with different characteristic widths (controlled by the index j) and centered in different spatial points (controlled by the index k). For functions defined on $N = 2^n$ points in the interval [0,1] the sums in (49) are restricted from zero to $n-1$ for the index j and from zero to $2^j - 1$ for k [37].

In [36] it has been shown that the statistical behavior of signal increments

$$\langle |\delta\phi(r)|^p \rangle = \langle |\phi(x+r) - \phi(x)|^p \rangle \sim r^{\zeta(p)}$$

is controlled by the coefficients $\alpha_{j,k}$. By defining the α coefficients in terms of a multiplicative random process on the diadic tree, it is possible to give an explicit expression for the scaling exponents $\zeta(p)$. For example, it is possible to recover the standard anomalous scaling by defining the α's tree in term of the realizations of a random variable η with a probability distribution $P(\eta)$:

$$\begin{aligned} &\alpha_{0,0} \\ &\alpha_{1,0} = \eta_{1,0}\alpha_{0,0}; \qquad \alpha_{1,1} = \eta_{1,1}\alpha_{0,0}; \\ &\alpha_{2,0} = \eta_{2,0}\alpha_{1,0}; \qquad \alpha_{2,1} = \eta_{2,1}\alpha_{1,0}; \\ &\alpha_{2,2} = \eta_{2,2}\alpha_{1,1}; \qquad \alpha_{2,3} = \eta_{2,3}\alpha_{1,1} \end{aligned} \tag{50}$$

and so on. Let us note that in the previous multiplicative process different scales are characterized by different values of the index j, i.e. $r_j = 2^{-j}$. If the $\eta_{j,k}$ are independent identically distributed (i.i.d.) random variable it is straightforward to realize that $\alpha_{j,k}$ are random variables with moments given by

$$\langle |\alpha_{j,k}|^p \rangle = r_j^{-\log_2(\overline{\eta^p})}, \tag{51}$$

where the "mother eddy" $\alpha_{0,0}$ has been chosen equal to one. In (51) with $\overline{\cdots}$ we intend averaging over the $P(\eta)$ distribution. In [36] it has been shown that also the signal $\phi(x)$ has the same anomalous scaling of (51).

In order to generalize this construction for functions showing ESS or generalized-ESS (G-ESS) scaling of the form (41) and (48) is now sufficient to take a probability distribution, $P_l(\eta)$, for the random multiplier with the appropriate scale dependency (25). This will be implemented by allowing a dependency of $P(\eta_{jk})$ on the scale $r_j = 2^{-j}$, i.e. the η's random variables will be still independently distributed but not identically distributed with respect to variation of the scaling index j.

According to the previous discussion, ESS corresponds to have only one seed-function defining the multiplicative process, i.e. $g_1(r)^{1/h_0} \neq g_2(r)^{1/d_0}$ in the range of scales where ESS is valid ($r \geq 5\eta_k$). On

the other hand, at scales smaller that 5–6 Kolmogorov scale, ESS is not more valid because g_2^{1/d_0} begins to deviate substantially from g_1^{1/h_0}: only G-ESS should be observed and we need a multiplicative process defined in terms of two differnt seed-functions.

Following this recipe we define the signal such that:

$$\langle \delta v(r)^p \rangle = U_0^p F(r)^{p/3} G(r)^{\zeta(p)-p/3}, \tag{52}$$

where

$$F(r) = \langle \delta v(r)^3 \rangle / U_0^3. \tag{53}$$

The function $G(r)$ is defined in such a way that for $F(r)$ much greater than η_k/L, $G(r) \sim F(r)$ while for very small scales r we have $G(r) \sim \eta_k/L$. In the following we choose the simplest ansatz:

$$G(r) = B + AF(r) \tag{54}$$

with $B = \eta_k/L$ and A is a dimensionless constant.

Let us now spend some words in order to clarify the previous definitions. Relation (52) is defined such that experimental results are reproduced with good accuracy and G-ESS scaling (48) is satisfied by definition. By assuming (54) the only unknown function is $F(r) = \langle \delta v(r)^3 \rangle / U_0^3$. On the other hand the function $\langle \delta v(r)^3 \rangle$ is always very well fitted by the Batchelor parameterization:

$$\langle \delta v(r)^3 \rangle = \frac{U_0^3}{L\eta_k^2} \frac{r^3}{(1 + (r/\eta_k)^2)}. \tag{55}$$

From expression (52) it is immediate to extract the expression for the two seed-functions $g_1(r)$, $g_2(r)$ used in the previous sections, namely:

$$g_1(r) = \left(\frac{F(r)}{G(r)}\right)^{1/3} G(r)^{h_0}, \qquad g_2(r) = G(r)^{d_0}. \tag{56}$$

Let us note that $g_1(r)$ goes smoothly from the intermittent value, $g_1(r) \sim r^{h_0} (h_0 = \frac{1}{9}$ for the case of She–Leveque model), assumed in the inertial range to the laminar value, $g_1(r) = \sim r$, characteristic of scales much smaller than Kolmogorov scale.

For the practical point of view we have constructed our signal by using a random process for the multiplier $\eta_{j,k}(r_j)$ with a scale-dependent log-Poisson distribution. The scale dependency of parameters entering the distribution has been fixed in terms of relations (56) and (29) and such that the $\zeta(p)$ exponents correspond to the She–Leveque [12] expression, namely:

$$\eta_{jk}(r_j) = A_{j,j+1} \beta^{x_{j,j+1}}, \tag{57}$$

where $x_{j,j+1}$ is a Poisson variable with mean $C_{j,j+1} = \log(g_2(r_j+1)/g_2(r_j))$, $A_{j,j+1} = g_1(r_j)/g_1(r_j+1)$ and $\beta = \frac{2}{3}$. This choice leads to the standard log-Poisson scaling in the inertial range

$$\zeta(p) = h_0 p + (1 - 3h_0) \frac{(1 - \beta^{p/3})}{(1 - \beta)}$$

and to the following expression for the ratios of deviations to the Kolmogorov law:

$$\rho_{p,q} = \frac{H(p) - p/3}{H(q) - q/3}, \qquad H(x) = \frac{1 - \beta^{x/3}}{(1 - \beta)}.$$

The signal constructed according to this scenario will be referred to as signal A in the following.

In Fig. 11 we show the structure function of order 6 for such a signal plotted versus the separation scale r at moderate Reynolds number. Clearly, for this choice of Reynolds number there is not any inertial range of scale where scaling exponents could be safely measured. On the other hand, our signal shows G-ESS scaling, as it is possible to see in Fig. 12.

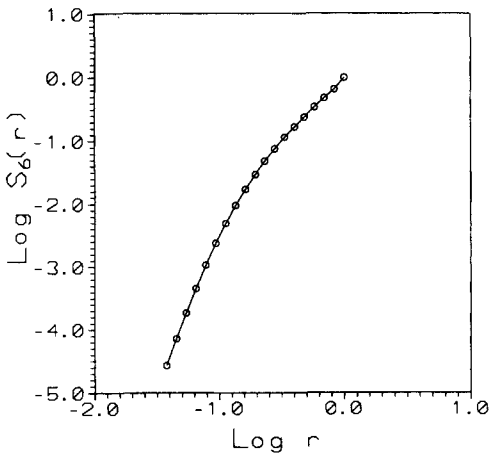

Fig. 11. Log–log plot of the sixth order structure function for the signal A with 19 fragmentation at small Reynolds number. Notice the absence of any scaling range.

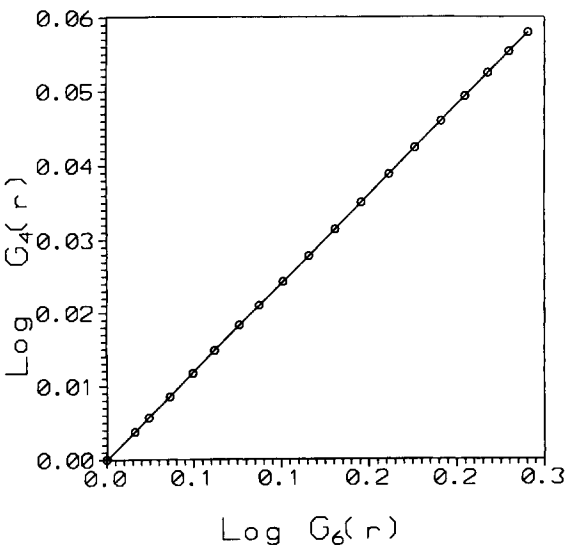

Fig. 12. G-ESS ($\log(G_4(r))$ versus $\log(G_6(r))$) for the signal A at the same Reynolds number of Fig. 11. The slope is $\rho_{4,6} = 0.241$ in perfect agreement with the theoretical prediction obtained from (18) where for $\zeta(p)$ we have used the She–Leveque expression.

7. Multiscaling

We now turn our attention to a different question which is connected to the theoretical results so far discussed, namely the role played by viscous effects. It is generally argued that the anomalous scaling can be observed for scales larger than a given viscous cutoff. The physical interpretation of this statement is that nonlinear, intermittent, transfer of energy is acting only for scales larger than the viscous scale. Below such a scale the structure functions are supposed to show a simple (regular) scaling $\langle \delta v^p(r) \rangle \sim r^p$.

Usually the viscous cutoff is introduced as the scale at which the local Reynolds number is of order 1, namely

$$\frac{\delta v(r) r}{\nu} \sim 1. \tag{58}$$

This condition can be obtained by the requirement that the local energy transfer $\varepsilon(r) \sim (\delta v^3(r)/r)$ becomes equal to the energy dissipation $\nu(\delta v^2(r)/r^2)$:

$$\nu \frac{\delta v^2(r)}{r^2} \sim \frac{\delta v^3(r)}{r}, \tag{59}$$

which gives Eq. (58). There is a well-defined prediction, based on (58), formulated by Frisch and Vergassola using the multifractal language. Indeed for any exponent h one can introduce the h-dependent viscous cutoff given by

$$r_{\mathrm{d}}^{h+1} \sim \nu, \tag{60}$$

where $\delta v(r) \sim r^h$.

It follows that $r_{\mathrm{d}}(h)$ is a fluctuating quantity. There are two consequences of this theory. The first one predicts that for the structure functions $\langle \delta v^p(r) \rangle$ there exists a cutoff scale r_p dependent on p and moreover $r_p < r_q$ for $p > q$.

The second prediction concerns the moment of the velocity gradients Γ which are

$$\langle \Gamma^p \rangle \sim \left\langle r_{\mathrm{d}}(h)^{(h-1)p} r_{\mathrm{d}}(h)^{3-d(h)} \right\rangle \sim \mathrm{Re}^{-z(p)} \tag{61}$$

with $z(p) = \sup_h[((h-1)p + 3 - D(h))/(1+h)]$.

Between the two predictions the first one is qualitatively more peculiar of (60).

In particular, the first prediction states that between the end of the inertial range (i.e. the region where anomalous scaling of $\langle \delta v^p(r) \rangle$ with respect to r is detected) and the dissipation cutoff r_{d}, the local slope is controlled in rather complicate way by $D(h)$. The second prediction is somehow weaker because present experimental data do not distinguish among several models, so far proposed, for the Re-dependence of $\langle \Gamma^p \rangle$.

In order to compare the multiscaling in the dissipation range with our experimental and numerical data, we have produced a synthetic turbulence signal (signal B hereafter) similar to the one already discussed but with d_0 and h_0 independent on r. The effect of dissipation is introduced is introduced by using (58). In Fig. 13 we compare the local scaling exponents $\mathrm{d}(\log\langle \delta v^p \rangle)/\mathrm{d}(\log r)$ for $p = 6$ between the two synthetic signals.

In Fig. 14 we plot the relation (45) for $p = 6$ for signal A and B. Finally in Fig. 15 we plot the ratio $G_4/G_6^{\rho_{4,6}}$ for signal B. By comparing Figs. 13–15 with the analogous experimental and numerical results discussed in the previous sections (see Figs. 5, 7 and 9), we can state that the quantitative and qualitative

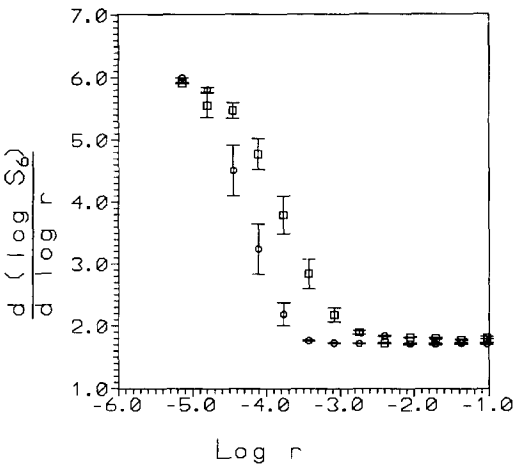

Fig. 13. Sixth order local scaling exponents for the signal A (□) and signal B (○). Notice that the qualitative behavior of the two signals is almost the same: both of them go from an intermittent scaling ($\zeta(6) \sim 1.8$) at large scale to a laminar scaling ($\zeta(6) = 6$) at small scales.

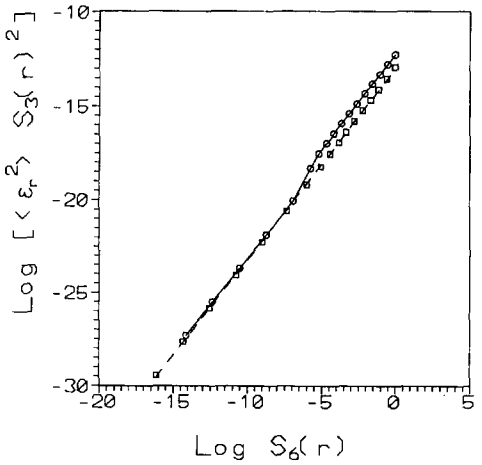

Fig. 14. Generalized-Kolmogorov refined hypothesis (45) for the sixth order structure function in both signal A (□) and signal B (○). Notice the sudden jump at the Kolmogorov scale present when multiscaling is valid (signal B).

prediction based on (60) is not verified by experimental data. On the other hand, signal A, based on an explicit r-dependence of d_0 and h_0, seems to be more closely related to what observed experimentally. Let us remark that signal A has no cutoff effect imposed by condition (58).

The above discussion rules out the effect of multiscaling on the viscous cutoff (60). Previous claims on

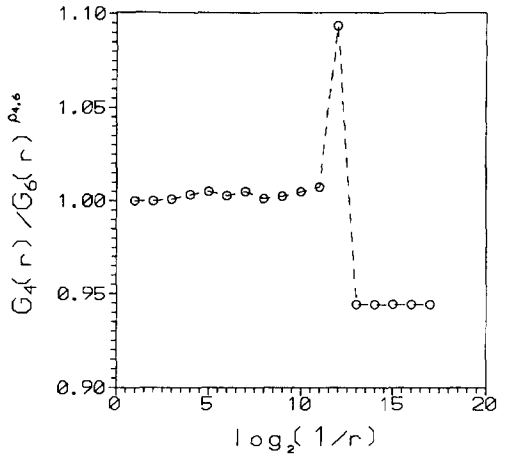

Fig. 15. Compensated slope $(G_4(r)/G_6^{\rho 4.6}(r))$ for signal B. Notice deviations of the order of 10% while for signal A the same quantity is constant by definition.

the validity of multiscaling effects should be considered either wrong or affected by experimental errors. On the other hand our model, used to implement the synthetic signal A, should be considered a very accurate model even for a scale close to the regular region where $\delta v(r) \sim r$.

There is, however, a theoretical question concerning multiscaling which we are still not able to answer completely and that we shall try to formulate in the following. There are two possible scenarios in which a viscous cutoff may be considered.

In the first scenario (let us call it scenario I) we can imagine to consider Eq. (58) as a fundamental relation independent of any other theoretical consideration. The idea is that when the local Reynolds number is sufficiently small, then nonlinear effects must be neglected. In order to compute the viscous scale, one shoud make use of the relation

$$\delta v(r) \sim U_0 F(r)^{1/3} G(r)^{h-1/3} \tag{62}$$

obtained by the two definitions (42) and (52). In Eq. (62) h is now the standard multifractal scale-independent exponent. Generalized scaling (62) should be considered realized with probability

$$P_h(r) \sim G(r)^{3-D(h)}. \tag{63}$$

Inserting (62) into (58) we obtain

$$r_d U_0 F(r_d)^{1/3} G(r_d)^{h-1/3} \sim \nu, \tag{64}$$

where $r_d(h)$ is the fluctuating cutoff.
We now look for a solution of Eq. (64) in a region where

$$F(r) \sim \frac{r^3}{L\eta_k^2}, \tag{65}$$

$$G(r) \sim \frac{\eta_k}{L}. \tag{66}$$

After some algebra we obtain

$$r_d(h) \sim \mathrm{Re}^{(3h-7)/8}. \tag{67}$$

Thus $r_d(h)$ is a fluctuating quantity as in (60). These fluctuations, however, happen in the region where $\delta v(r) \sim r$ and therefore, no effect on the scaling of structure function is produced. From (62)–(65) we can compute the scaling of $\langle \Gamma^p \rangle$ as function of Re. The scaling is independent on $r_d(h)$ and it is

$$\langle \Gamma^p \rangle \sim \mathrm{Re}^{(3/4)(p-\zeta_p)}, \tag{68}$$

consistent with (62) in the limit $r \to 0$. Note that $\langle \Gamma^2 \rangle \sim \mathrm{Re}^{(3/4)(2-\zeta_2)}$. This implies that for $\zeta_2 \neq \frac{2}{3}$, $\langle \Gamma^2 \rangle$ does not scale as Re. If we want to recover the experimental fact that $\langle \varepsilon \rangle$ is constant with Re, we should allow for a Re-dependent constant in (62). At any rate, because $\zeta_2 - \frac{2}{3}$ is a small quantity, these effects are quite small in the full range of available Re-number.

We can summarize the scenario I as follows: the scaling (48) and (62) are verified to all scales; the condition (58) introduces a viscous cutoff which fluctuates in the region where $\delta v(r) \sim r$; intermittency in the gradient of the velocity field are prescribed by (62).

The above conclusions imply that scaling (45) must be violated near the viscous cutoff, as one can immediately check by an explicit computation. One can take an opposite point of view and assume that (45) is a fundamental relationship which must not be violated. This corresponds to the second scenario.

In the second scenario (58) is disregarded and one generalizes (59) as

$$\nu \Gamma^2 \sim \frac{\delta v^3(r_d)}{\langle \delta v^3(r_d) \rangle} \varepsilon, \tag{69}$$

where Γ is the velocity gradient and r_d is the viscous cutoff. In order to compute r_d, one observes that $\Gamma \sim 1/\tau(r_d)$ where $\tau(r_d)$ is the eddy turnover time at the viscous cutoff. We obtain

$$\nu \sim \frac{\delta v^3(r_d)\tau(r_d)^2}{\langle \delta v^3(r_d) \rangle} \sim \frac{\delta v(r_d)\langle \delta v^3(r_d) \rangle}{\varepsilon}, \tag{70}$$

where following (46), we used $\tau r_d \delta v(r_d) = \langle \delta v^3(r_d) \rangle / \varepsilon$. Once again, by using (62), (65) and (66) we can obtain an explicit formula for $r_d(h)$

$$r_d(h) \sim \mathrm{Re}^{-(3/16)(13/3-h)} \eta_k. \tag{71}$$

Thus also in scenario II, we have strong fluctuations of the viscous cutoff.

The computation of the gradients is quite straightforward from (69). We have

$$\Gamma \sim \mathrm{Re}^{1/2} \left(\frac{\delta v^3(r)}{\langle \delta v^3(r) \rangle} \right)^{1/2} \sim \mathrm{Re}^{1/2} G(r_d)^{(3h-1/2)}, \tag{72}$$

where we have used (62). Finally by using (63) and (66) we get

$$\begin{aligned} \langle \Gamma^p \rangle &= \mathrm{Re}^{p/2} G(r_d)^{(\zeta_{3p/2}-p/2)} \\ &\simeq \mathrm{Re}^{p/2}\, \mathrm{Re}^{3/4(\zeta_{3p/2}-p/2)}. \end{aligned} \tag{73}$$

Note that in scenario II $\langle \Gamma^2 \rangle \sim \mathrm{Re}$ because $\zeta_3 = 1$. Because of (73), the II scenario violates (62) and (48) for scales smaller than $r_d(h)$ while (45) is always satisfied.

It is quite difficult to understand which one of the two scenarios is actually verified by experimental and numerical data. In most cases the scale resolution does not reach the region where $\delta v(r) \sim r$. At any rate, either (45) or (48) should be violated at very small scales as the result of viscous effects. This violation is rather small and may not be easily detectable at low or moderate Reynolds numbers. The common point about the two scenarios is that the viscous cutoff (if any) acts at a scale where already the velocity structure functions behave in a regular way, i.e. $\delta v(r) \sim r$.

8. Conclusions

In this paper we proposed several new results concerning the scaling behavior of small scale statistical properties of turbulence. It is worth to summarize our main findings trying to outline questions which are still to be answered.

(1) We have reviewed the main results on ESS and in particular we have shown that in homogeneous and isotropic flows in turbulence, Rayleigh–Benard convection and solar wind magnetohydrodynamics, the ratio $\zeta(p)/\zeta(3)$ seems to have an universal behavior. This is a rather striking and unexpected result which implies that anomalous violation of dimensional scaling may be explained in an universal way. We do not know any simple phenomenological explanation for our finding.

(2) We have shown that ESS is not observed when relatively strong shear flows are present. A phenomenological analysis, based on the Kolmogorov equation, shows the relevance of a length scale based on the mean energy dissipation and the shear strength. This analysis should be refined in order to acquire more quantitative predictions. At any rate, our observation suggests that previous finding of violations of ESS should be due to the presence of shear flows.

(3) We have shown that the refined Kolmogorov similarity can be generalized by including ESS. This generalization is verified extremely well in both experiments and numerical simulations. More important, we have shown that the generalized refined Kolmogorov similarity is true also in cases where ESS is not observed.

(4) Similar to the previous point, we have shown that the hierarchy relation based on log-Poisson distribution for the structure functions is very well supported by experimental data, also for very small scales where ESS is not observed. In the Appendix A we have also shown that this extention of the hierarchy to all scales is not a general feature of any turbulent field, but it is a property of the velocity field, which plays an important role in our theoretical interpretation.

(5) Based on our results in (1)–(4) we have proposed a generalization of ESS. This generalization is supported both by experimental and numerical data and it seems not affected by viscous cutoff.

(6) We developed a theory which unifies the previous point. The theory is based on the assumption that the probability distribution is infinitely divisible and predicts the existence of the G-ESS. The theory can also be used to generate artificial signals which displays all the scaling features observed in real data.

(7) We have shown that the original proposal on the multiscaling for the viscous cutoff is incompatible with the turbulence data. The theory formulated in this paper removes this incompatibility and suggests that multiscaling is acting at much smaller scales than previously proposed. The new point on the theory is a change of view in the probability distribution of the original multifractal model which is not directly linked to a geometrical interpretation in terms of fractal dimensions.

(8) Finally we have shown that violations of either the generalized refined Kolmogorov similarity or the G-ESS should occur at very small scale. Our present data analysis does not allow us to distinguish among the two possibilities.

Acknowledgements

We thank B. Castaign, S. Fauve, U. Frisch, Z.S. She, K.R. Sreenivasan and G. Stolovitzky, for many useful discussions. During the writing of this paper, we became aware of a manuscript of C. Meneveau dealing with a possible explanation of ESS. His conclusions are physically close to part of the discussion in Section 6.

This work has been partially supported by EEC contracts ERBCHBICT941034, CT93-EVSV-0259 and CHRX-CT94-0546.

Appendix A

In Section 4 we have shown that the hierarchy relation for the velocity structure functions, Eq. (14),

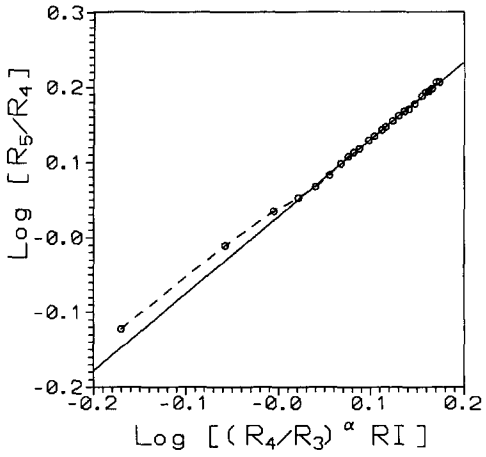

Fig. 16. Hierarchy of the structure functions of a passive scalar transported by a turbulent flow at $\mathrm{Re} = 50\,000$, $\alpha = 0.62$. The straight line has a slope 1.02.

has the property of being satisfied from large to small scales. In this appendix we want to point out that this property, which has very important consequences in our theoretical interpretation of Section 6, is not a generic feature of any turbulent field. As an example we consider the structure functions $R_n(r)$ of a passive scalar for which ESS is observed [19]. One can check if the following hierarchy (which is similar to Eq. (14) for the velocity structure functions) is supported by the experimental data [38]:

$$\frac{R_{n+1}(r)}{R_n(r)} \propto \left(\frac{R_n(r)}{R_{n-1}(r)}\right)^{\alpha} RI(r), \tag{A.1}$$

where $RI(r) \propto R_2(r)/R_1(r)^{1+\alpha}$. Eq. (A.1) has been checked [38] by using the experimental measurements of a temperature field passively transported by a tubulent flow [19]. In Fig. 16 we report in log–log scale $R_6(r)/R_5(r)$ versus $(R_5(r)/R_4(r))^{\alpha} RI(r)$ with $\alpha = 0.62$ (this value has been experimentally determined). We see that the dissipative and inertial range both present a slope of 1, showing that Eq. (A.1) is satisfied in both regions. However, the transition between these two regions is characterized by a jump, which is not observed in the case of the velocity structure functions (compare Fig. 16 with Fig. 8). This example clearly shows that a hierarchy similar to Eq. (14) does not necessarily extend to all scales. This very important feature of the velocity field plays a key role in our theoretical interpretation in Section 6.

References

[1] A.S. Monin and A.M. Yaglom, Statistical Fluid Mechanics (MIT Press, Cambridge, MA, 1975).
[2] A.N. Kolmogorov, C.R. Acad. Sci.USSR, 30 (1941) 299.
[3] F. Anselmet, Y. Gagne, E.J. Hopfinger and R.A. Antonia, J. Fluid Mech. 140 (1984) 63.
[4] A. Vincent and M. Meneguzzi, J. Fluid Mech. 225 (1991) 1.
[5] A.N. Kolmogorov, J. Fluid Mech. 13 (1962) 83.
[6] U. Frish, P. Sulem and M. Nelkin, J. Fluid Mech. 87 (1978) 719.
[7] G. Parisi and U. Frish, On the singularity structure of fully developed turbulence, in: Turbulence and Predictability in Geophysical Fluid Dynamics and Climate Dynamics, eds. M. Ghil, R. Benzi and G. Parisi (North-Holland, Amsterdam, 1985) p. 84.
[8] R. Benzi, G. Paladin, G. Parisi and A. Vulpiani, J. Phys. A 17 (1984) 3521.
[9] C. Meneveau and K.R. Sreenivasan, Phys. Rev. Lett. 59 (1987) 1424.
[10] Y. Gagne and B. Castaing, C.R. Acad. Sci. Paris 312 (1991) 441.
[11] B. Castaing, Y. Gagne and E. Hopfinger, Physica D 46 (1990) 177.
[12] Z.S. She and E. Leveque, Phys. Rev. Lett. 72 (1994) 336.
[13] U. Frish and M. Vergassola, Europhys. Lett. 14 (1991) 439.
[14] R. Benzi, S. Ciliberto, R. Tripiccione, C. Baudet and S. Succi, Phys. Rev. E 48 (1993) R29.
[15] R. Benzi, S. Ciliberto, C. Baudet and G. Ruiz Chavarria, Physica D 80 (1995) 385.
[16] G. Stolovitzky and K.R. Sreenivasan, Phys. Rev. E 48 (1993) 32.
[17] M. Briscolini, P. Santangelo, S. Succi and R. Benzi, Phys. Rev. E 50 (1994) 1745.
[18] R. Benzi, R. Tripiccione, F. Massaioli, S. Succi and S. Ciliberto, Europhys. Lett. 25 (1994) 331.
[19] G. Ruiz Chavarria, C. Baudet and S. Ciliberto, ESS in passive scalars, in Europhys. Lett., to be published.
[20] S. Cioni, S. Ciliberto and J. Sommeria, Scaling laws in turbulent thermal convection in low Prandtl number fluids, Europhys. Lett., to be published.
[21] R. Grauer, Physics Lett. A 195 (1994) 335.
[22] F. Belin, P. Tabeling and H. Willaime, Exponents of structure functions in a low temperature helium experiment, Physica D, submitted.
[23] G. Ruiz Chavarria, J. Physique 4 (1994) 1083.
[24] G. Ruiz, Scaling law in boundary layer turbulence, in preparation.
[25] R. Benzi, S. Ciliberto, C. Baudet, G. Ruiz Chavarria and R. Tripiccione, Europhys. Lett. 24 (1993) 275.
[26] R. Benzi, M.V. Struglia and R. Tripiccione, ESS in numerical simulations of 3D anisotropic turbulence, preprint (1995), submitted.

[27] G. Ruiz Chavarria, C. Baudet, R. Benzi and S. Ciliberto, J. Physique 5 (1995) 485.
[28] G. Ruiz Chavarria, C. Baudet and S. Ciliberto, Phys. Rev. Lett. 74 (1995) 1986.
[29] G. Amati, R. Benzi and S. Succi, in preparation.
[30] Feller, An Introduction to Probability Theory and its Applications, Vol. 2 (Wiley, New York, 1966).
[31] E.A. Novikov, Phys. Rev. E 50 (1994) R3303.
[32] B. Dubrulle, Phys. Rev. Lett. 73 (1994) 959.
[33] Z.-S. She and E.C. Waymire, Phys. Rev. Lett. 74 (1995) 262.
[34] B. Castaing and B. Dubrulle, J. Phys. II France 5 (1995) 895.
[35] B. Castaing, The temperature of turbulent flows, J. Physique, to be published.
[36] R. Benzi, L. Biferale, A. Crisanti, G. Paladin, M. Vergassola and A. Vulpiani, Physica D 65 (1993) 352.
[37] Y. Meyer, Actualité Mathematiques (Hermann, Paris, 1990).
[38] G. Ruiz, C. Baudet and S. Ciliberto, Passive scalar properties in fully developed turbulence, in preparation.